Macromolecules

ARTICLE

pubs.acs.org/Macromolecules

Size-Controlled Polymer-Coated Nanoparticles as Efficient Compatibilizers for Polymer Blends

Taegyun Kwon,[†] Taesu Kim,[†] Fathilah binti Ali,[†] Dong Jin Kang,[†] Misang Yoo,[‡] Joona Bang,[‡] Wonbo Lee,[§] and Bumjoon J. Kim*[,†]

[†]Department of Chemical and Biomolecular Engineering, Korea Advanced Institute of Science and Technology (KAIST), Daejeon 305-701, Republic of Korea

[‡]Department of Chemical and Biological Engineering, Korea University, Seoul 136-701, Republic of Korea

[§]Department of Chemical and Biomolecular Engineering, Sogang University, Seoul 121-742, Republic of Korea

Supporting Information

ABSTRACT: Polymer-coated gold nanoparticles (Au NPs) with controlled size and surface chemistry were successfully synthesized and applied to tailor the structures and properties of polytriphenylamine (PTPA) and polystyrene (PS) blends. Two different polymer-coated Au NPs with sizes of 5.9 nm (Au NP-1) and 20.7 nm (Au NP-2) were designed to be thermally stable above 200 °C and neutral to both PS and PTPA phases. Hence, both Au NPs localize at the PS/PTPA interface and function as compatibilizers in the PS/PTPA blend. To show the compatibilizing effect of the particles, the morphological behaviors of PS/PTPA blends containing different particle volume fractions (ϕ_p) of Au NPs were observed using cross-sectional TEM, and for quantitative analysis, the size distribution of PTPA droplets in the PS matrix was obtained for each sample. The number-average droplet diameter (D_n) of the PTPA domain in the blend was dramatically reduced from 1.4 μm to 500 nm at a small ϕ_p of 1.0 vol % Au NP-1. The same trend of decreasing D_n was also observed with the addition of larger Au NP-2, but a higher ϕ_p was required to obtain the same amount of reduction in the PTPA droplet size. The ϕ_p required to fully cover the PS/PTPA interface as a packed monolayer of Au NPs was calculated as 0.98 vol % for Au NP-1 and 3.38 vol % for Au NP-2, thus giving excellent agreement with critical ϕ_p values for the saturation of the PTPA droplet diameter D_n. To demonstrate the effectiveness of Au NPs as compatibilizers, polystyrene-*b*-poly(triphenylamine) (PS-*b*-PTPA) block copolymers were also synthesized and used as compatibilizers in the PS/PTPA blend. The decrease in D_n with the addition of PS-*b*-PTPA was always smaller than that with addition of Au NP-1 at the same ϕ_p, indicating that Au NPs are more effective compatibilizers. This different behavior can be attributed to the presence of PS-*b*-PTPA compatibilizers as micelles or free chains in the homopolymer matrix. In contrast, most Au NPs were strongly adsorbed to the PS/PTPA interface.

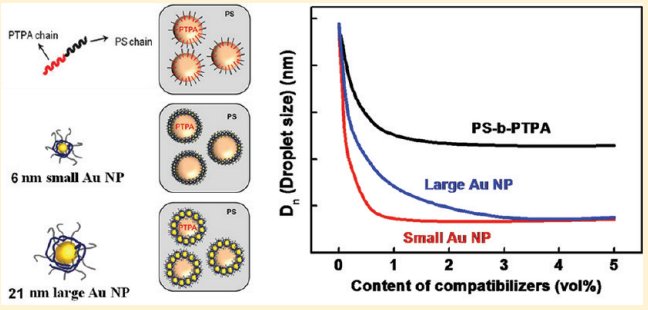

INTRODUCTION

Polymer blends containing conducting polymers have attracted a great deal of interest in various applications, including membranes, barriers, and optoelectronic devices such as polymer solar cells and LEDs.[1−8] However, conducting polymers usually suffer from low processability, low mechanical strength, and high cost due to their low solubility. For applications such as organic electronics and coatings, which require both conductivity and good mechanical strength, one good approach involves blending the conducting polymer with a lower cost matrix polymer that provides the desired mechanical properties without interfering with the unique features of the conducting polymer, such as its electrical and optical properties.[5−7] However, simple blending usually does not allow a high degree of morphological control because the entropy of mixing is generally low for polymers; i.e., solid polymer blends tend to be phase-separated at the macroscopic scale.

Block and graft copolymers have been widely used as compatibilizers for improving miscibility in polymer blends.[9−18] The addition of compatibilizers to polymer blends reduces the interfacial tension and phase coarsening rate, thus hindering macrophase separation and stabilizing the desired morphology. However, because copolymer stabilizers often form micelles within one of the blended materials, the use of premade copolymers is impractical. In addition, although the removal of copolymer surfactants is important for many applications

Received: September 3, 2011
Revised: October 31, 2011
Published: December 01, 2011

Scheme 1. (a) Schematic Representation of Experimental System (Small Au NP-1, Large Au NP-2 and PS-*b*-PTPA) and the Application in a PS/PTPA Blend; (b) Synthetic Schemes for PS-*b*-PTPA Block Copolymers and PS-*b*-PSN$_3$-SH Ligands

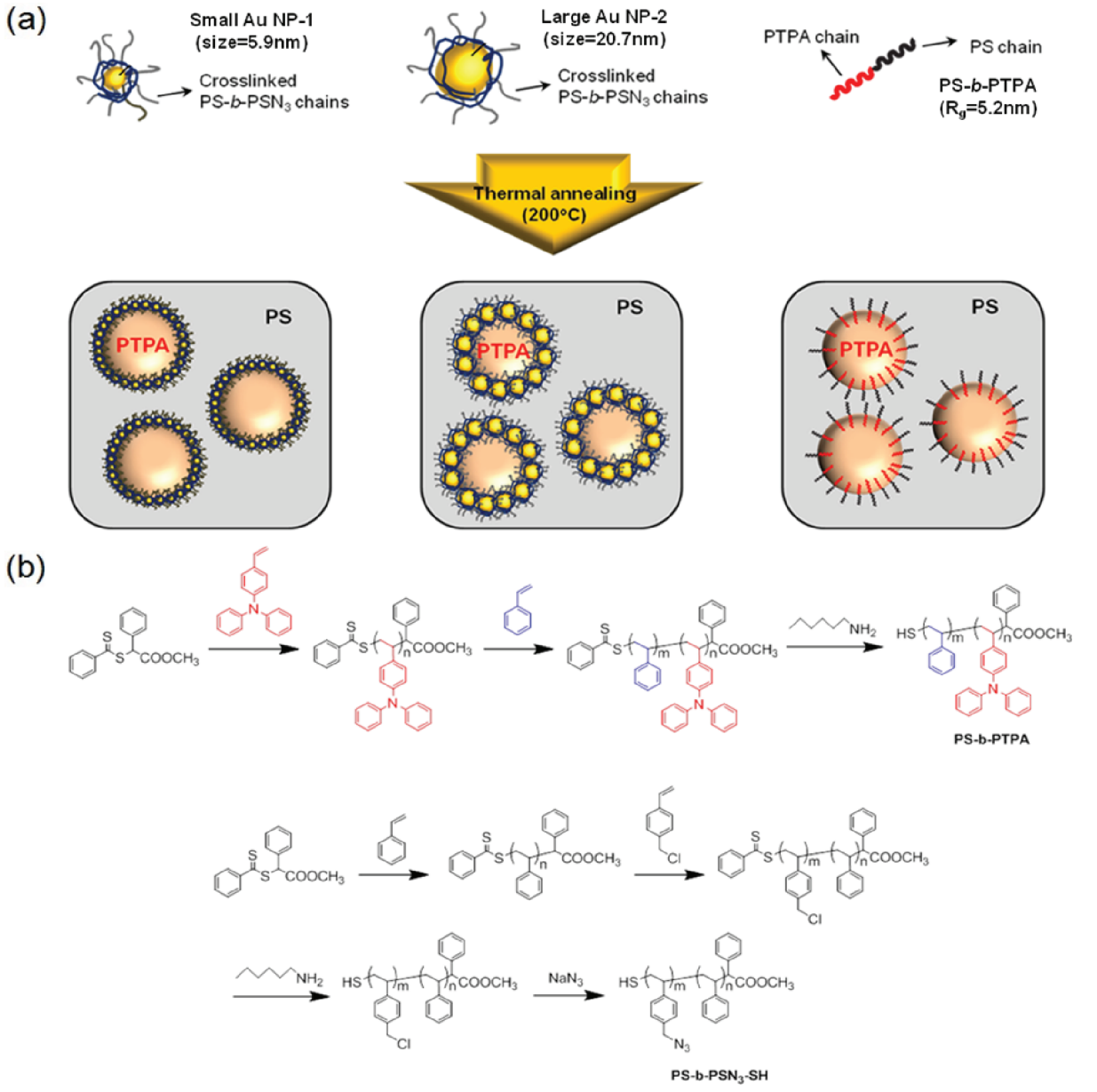

because they affect the properties of the resulting polymer, they are difficult and costly to remove.[19]

Nanoparticles (NPs) can be used as an alternative means that may be more generally applicable and provide additional opportunities to tailor the properties of the polymer blends. In comparison to conventional emulsions that are stabilized by surfactants, particle-stabilized emulsions are extremely stable because of the quasi-irreversible adsorption of particles to the interface.[20−23] Recently, NP surfactants, using titania and silica NPs whose surfaces are modified with oleic acid, have been demonstrated to help create emulsions by preventing coalescence.[24−27] In addition, NPs have been used to enhance the morphology of polymer blends.[28−34] For example, Elias et al. reported the use of silica NPs as compatibilizers in polypropylene/polystyrene blends and studied their effects on the rheological and morphological properties of the blends.[28,30] Interestingly, Chung et al. observed that the interfacial segregation of silica NPs stabilized a bicontinuous structure for blends of poly(methyl methacrylate) and poly(styrene-*r*-acrylonitrile).[32] While these works demonstrate the importance of NPs as surfactants, the effectiveness of NPs as surfactants can be limited because of the often ill-defined state of NP dispersion and surface properties. Moreover, in these studies, the localization of NPs at the interface was not accurate, and their size and surface chemistry were not systemically controlled. In particular, a system including NPs with controlled surface properties and structure is needed to control NP location and dispersion in the polymer matrix.[33,34]

The most promising strategy is to control the enthalpic interaction between the polymer matrix and inorganic NPs through tailoring the surface properties of NPs by end-attaching of polymer ligands to the NP surface.[35−48] It should be noted

that the adsorption energy of NPs onto the interface, which determines the ability of the NPs to serve as a surfactant, is strongly dependent on the enthalpic interaction between the NP surface and the polymer matrix. For example, Au NPs stabilized by various thiol-terminated polymer ligands have been used to precisely control the location of NPs to one domain or to the interface between domains of diblock copolymers.[40−42] Au NPs are considered as model inorganic NPs for the study of the interaction between NPs and polymer matrix for the following reasons. First, the surface properties of Au NPs can be easily controlled through the facile grafting of thiol end groups to obtain a surface with polymer ligands at a controlled areal density, which is a critical parameter for producing NP surfactants for various polymer and/or fluid mixtures.[40,49,50] Second, the strong contrast between Au NPs and polymers under electron microscopy, as well as their ability to absorb light in the visible spectrum, makes them well suited for model studies on the effect of NPs in compatibilizing polymer blends. In addition, through judicious selection of the polymer shell, polymer-coated Au NPs can have high thermal stability, which makes them perfectly suited for polymer blending requiring high-temperature processing.[51,52]

In this work, we developed a model system of polymer-coated Au NPs with controlled sizes of 5.9 nm (Au NP-1) and 20.7 nm (Au NP-2) and a uniform size distribution and employed these NPs as compatibilizers in immiscible PS and conducting PTPA polymer blends. (Scheme 1) The Au NPs were coated by carefully designed thiol-terminated polystyrene-*b*-poly(4-azidostyrene) (PS-*b*-PSN_3) block copolymers, making them thermally stable above 200 °C and ensuring neutral interactions between the PS and PTPA domains. To elucidate the role of Au NP compatibilizers and quantitatively determine their compatibilizing effects, Au NP-1 and Au NP-2 with two different sizes were utilized, and their compatibilizing effects were compared with that of polystyrene-*b*-poly(triphenylamine) (PS-*b*-PTPA) block copolymers. To the best of our knowledge, this is the first systematic study of the effects of the size of NP compatibilizers on a polymer blend. The morphology of PS/PTPA blends containing Au NPs with different particle volume fractions (ϕ_p) was observed using cross-sectional TEM; for quantitative analysis, the statistical distribution of the number-average PTPA droplet size (D_n) in the PS matrix was compared. In addition, PS-*b*-PTPA block copolymers were synthesized and used as compatibilizers in the PS/PTPA blend for the control sample. Scheme 1 illustrates the experimental system showing three different compatibilizers of Au NP-1, Au NP-2, and PS-*b*-PTPA as well as the structure of the polymers used in this study.

EXPERIMENTAL SECTION

Synthesis of 4-Vinyltriphenylamine Monomer (VTPA). 4-Bromostyrene, diphenylamine, and sodium *tert*-butoxide (NaO-*t*-Bu, 97%) were dissolved in toluene, and $Pd(dba)_2$ and tri-*tert*-butylphosphine ($P(t\text{-}Bu)_3$, 98%) were added under a nitrogen (N_2) atmosphere. The reaction mixture was stirred at room temperature for 1 h, acidified with HCl, and washed with dichloromethane (DCM). The mixture was purified by chromatography using eluent with a gradient composition of 1:4 DCM:hexane to 1:15 DCM:hexane to yield white solid products, followed by solidification in vacuum for 2 days (yield = 89%). ^{1}H NMR ($CDCl_3$, 300 MHz) δ (ppm): 7.3−7.22 (m, 6H, Ar), 7.09 (d, J = 7.6 Hz, 4H, Ar), 7.04−7.00 (m, 4H, Ar), 6.67 (q, J = 6.7 Hz, 1H, vinyl), 5.64 (d, J = 17.1 Hz, 1H, vinyl), 5.15 (d, J = 10.9 Hz, 1H, vinyl).

Table 1. Characteristics of Polymers Used in This Study

list	M_n (kg/mol)	M_w/M_n	f_{PS}
PS-*b*-PSN_3	2.4	1.19	0.79
PS	47	1.12	
PTPA	46	1.18	
PS-*b*-PTPA	54	1.23	0.50

Table 2. Characteristics of Polymer-Coated Au NPs Used in This Study

list	⟨core diam⟩ (nm)[a]	(core + shell) diam (nm)	Σ (chains/nm^2)
Au NP-1	2.7 ± 0.3	5.9	1.1
Au NP-2	12.3 ± 1.1	20.7	2.0

[a] Analysis obtained from TEM images.

Synthesis of Polystyrene (PS), Polytriphenylamine (PTPA), and PS-*b*-PTPA Block Copolymer. PS homopolymers were synthesized via the living radical polymerization of reversible addition−fragmentation transfer (RAFT) method.[53−56] The RAFT chain transfer agent (CTA), methyl-2-phenyl-2-(phenylcarbonothioylthio)acetate, was prepared following a procedure as described elsewhere.[53] The reaction mixture was degassed by three freeze−pump−thaw cycles. The reaction was carried out at 70 °C for 24 h under vacuum followed by precipitation using cold methanol. The molecular weight (M_n) and polydispersity index (PDI) of PS were 47 kg/mol and 1.12, respectively. PTPA homopolymers were also synthesized using the procedure described above. The M_n and PDI of PTPA were 46 kg/mol and 1.18, respectively. PS-*b*-PTPA diblock copolymers were also synthesized by RAFT polymerization. The M_n and PDI of PS-*b*-PTPA were 54 kg/mol (27 and 27 kg/mol) and 1.23, respectively (Figure S1) The M_n as well as the PDI of the polymers was measured by size exclusion chromatography (SEC) with calibration using a PS standard. To eliminate the end group of the RAFT agent, the polymers were dissolved in toluene with AIBN using a molar ratio of polymer to AIBN of 1:20. After purging with nitrogen for 10 min, the solution was reacted at 80 °C for 2.5 h and then precipitated using cold methanol to form a white product.

Synthesis of Thiol-Terminated Polystyrene-*b*-poly(4-azidostyrene) (PS-*b*-PSN_3) Block Copolymers. Thiol-terminated PS-*b*-PSN_3 block copolymers were synthesized by RAFT polymerization at 70 °C using dithioester RAFT agent and AIBN as reported in our previous studies.[51,57] The PS block was polymerized and then precipitated in cold methanol. Then, 4-chlorostyrene monomer was added to the PS polymers to produce the second block of poly(4-chlorostyrene). The polymer end group was converted to a thiol group by reaction with hexylamine, and then an azide group was subsequently introduced by reaction with sodium azide. The total M_n and PDI of PS-*b*-PSN_3 were determined to be 2.4 kg/mol and 1.12 by SEC, where the M_n of PS and PSN_3 block were 1.9 and 0.5 kg/mol. Information on the polymers used in this study is summarized in Table 1.

Synthesis of Small Size PS-*b*-PSN_3-Coated Au NPs (Au NP-1). The synthesis of PS-*b*-PSN_3-coated Au NPs was accomplished using a two-phase method consisting of toluene and water, as described elsewhere.[58] The initial molar feed ratio of PS-*b*-PSN_3 ligands to (Au atoms + PS-*b*-PSN_3 ligands) was 1:2.6. The characteristics of the polymer-coated Au NPs are summarized in Table 2. Ungrafted polymer ligands were carefully washed several times by centrifugation using the density-gradient method; in this method, the particles were washed through five different layers of DCM (ρ = 1.33 g/cm^3) and cyclohexane (ρ = 0.78 g/cm^3) at various ratios with different densities.[59] The unwashed polymers were monitored by SEC after each washing step. From SEC measurement, complete purification was verified by the fact

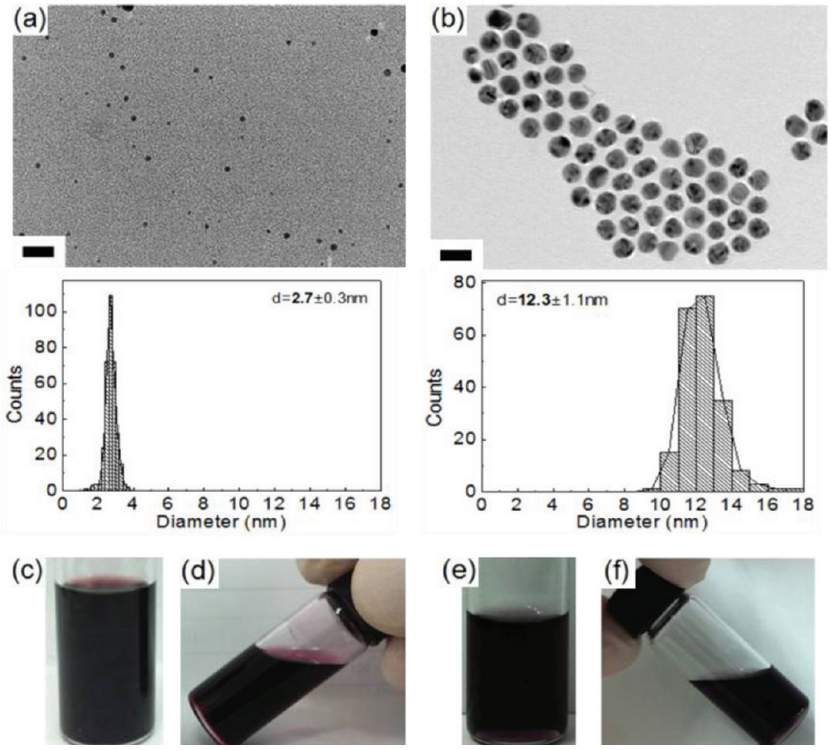

Figure 1. TEM images of two different (PS-*b*-PSN_3)-Au NPs and corresponding histograms of their size distributions; the NPs shown have average core diameters of (a) 2.7 nm (Au NP-1) and (b) 12.3 nm (Au NP-2). Scale bar is 20 nm. The lower left part of the figure shows photographic images of Au NP-1 in DBP solution (c) before and (d) after thermal stability test; the lower right portion shows Au NP-2 in DBP solution (e) before and (f) after thermal stability test. Thermal stability tests were conducted by heating Au NPs in DBP solution at 150 °C for 24 h. The particles were dispersed without any aggregation.

that no peak was observed at the molecular weight of the corresponding ungrafted polymeric ligands (Figure S2). The areal chain density (Σ) and shell thickness of the polymers on the surface of the Au NPs were calculated to be 1.1 chain/nm^2 and 1.6 nm, respectively. These values are based on the Au core size, which was determined using TEM, and on the relative weights of the Au core and the polymer ligands in the Au NP-1, which was determined using thermogravimetric analysis (TGA) as described elsewhere.[40]

Synthesis of Large Size PS-*b*-PSN_3-Coated Au NPs (Au NP-2). Large size Au NPs with a core diameter of 12.3 nm were synthesized using trisodium citrate (Aldrich, 98%) as surfactant in aqueous phase, similar to the previous report.[60] The initial feed molar ratio of PS-*b*-PSN_3 ligands to (Au atoms + PS-*b*-PSN_3 ligands) was 1:2. After vigorous stirring of the solution for 1 day under a N_2 atmosphere, the color of the toluene phase changed from transparent to wine red, while the color in the water phase disappeared, indicating complete phase transfer of Au NPs by efficient coating of PS-*b*-PSN_3 ligands on the particle surfaces. And PS-*b*-PSN_3-coated Au NPs were concentrated from toluene and washed using methanol three times to remove any unwashed residue including citrate residue. The ungrafted polymer ligands were then carefully washed several times by centrifugation at 20 000 rpm using the density-gradient method described in the previous section. Because Au NP-2 was too large to flow through the SEC column, the unwashed polymer ligands were monitored by TGA after each washing step to confirm their complete washing. Washing was continued until the ratio of inorganic core to organic shell showed no changes in TGA. The obtained Au NPs were then characterized by TEM and TGA.

Preparation of PS/PTPA/Au NPs Composites. The nanocomposite samples were prepared by mixing PS and PTPA homopolymers with Au NP-1 or Au NP-2 in DCM. The volume ratio of PS to PTPA in the blend was maintained at 8:2 to produce a homogeneous morphology of PTPA droplets in the PS matrix. The volume fraction of the Au NPs in the blend of PS/PTPA/Au-NPs was varied from 0 to 5.0 vol % to examine the effect of compatibilizer concentration on the polymer blend. The polymer/NPs composites were prepared by solvent-casting their solution onto a NaCl substrate with slow solvent evaporation. Then, the film was thermally annealed at 200 °C for 48 h under ultrahigh vacuum ($<10^{-6}$ Torr) to prevent degradation or oxidation. The annealing temperature used is much higher than the glass transition temperatures (T_g) of both polymers (i.e., PS $T_g \sim 100$ °C, PTPA $T_g \sim 130$ °C). To characterize the morphology of these nanocomposites by cross-sectional TEM, TEM samples were prepared. First, polymer/NPs composite films were floated from the NaCl substrate and transferred to epoxy supports, and the epoxy-supported thick films were cured in an oven at 60 °C for 24 h. The epoxy-supported thick films were then microtomed with a diamond knife at room temperature into 50 nm slices. The sections were floated on distilled water and collected on 200 mesh carbon film-coated copper grids. To characterize the morphology of the PS-*b*-PTPA polymers by scanning force microscopy (SFM), the PS-*b*-PTPA film was prepared by solvent-casting its solution onto a NaCl substrate with slow solvent evaporation. The film was then thermally annealed at 200 °C for 48 h under ultrahigh vacuum ($<10^{-6}$ Torr), floated from the NaCl substrate, and transferred to an epoxy support. The epoxy-supported thick film was cured in an oven at 60 °C for 24 h. The cured epoxy-supported thick film was microtomed into 50 nm slices using a diamond knife. The sectioned slices were floated on distilled water and collected on Si substrate, followed by drying under vacuum for 4 h. To enhance the contrast between PS and PTPA domains, the film was treated by O_2 plasma etching.

dx.doi.org/10.1021/ma2020134 |*Macromolecules* 2011, 44, 9852–9862

Characterization. The size of PS-*b*-PSN_3-coated Au NPs as well as the location of these particles in the PS/PTPA blend was determined by TEM (JEOL 2000FX) operated at 200 kV. The Au NPs were dissolved in DCM at a very low concentration. A 20−30 nm thick carbon film-coated TEM grid was dipped into the solution for a second, dried in the air, and examined by TEM. The size distribution of PTPA droplets in PS blend was obtained by image analysis of TEM images covering at least 300−400 units of droplets per sample. The structural information on the PS-*b*-PTPA diblock copolymers was obtained by small-angle X-ray scattering (SAXS) experiment. For SAXS measurement, 1 mm thick PS-*b*-PTPA films were prepared using a mold, followed by annealing at 200 °C for 48 h under nitrogen and slow cooling to room temperature. SAXS measurements using an X-ray wavelength of 1.54 Å were performed on beamline 4C1 in the Pohang Accelerator Laboratory (PAL), Korea. The surface morphology of the PS-*b*-PTPA films was examined using SFM measurement (Veeco Dimension 4100) in tapping mode.

RESULTS AND DISCUSSION

NPs can act as surfactant molecules when they are adsorbed onto an immiscible polymer−polymer interface. In a composite system of brush-grafted particles and homopolymers with athermal interaction, particle sizes affect miscibility due to curvature effect that grafted polymers at high curvature have less neighbors.[61] However, for our case (i.e., a composite system of brush-grafted particles and two homopolymers), enthalpic interactions are dominant, which leads to strong localization of NPs at the interface, thereby reducing interfacial energy cost.[62] Particle surfactants have been demonstrated to help create emulsions by decreasing the interfacial tension and stabilizing the film between droplets, thus preventing coalescence.[20,63] Such a surfactant effect should be strongly dependent on the particle size.[62,64] However, to the best of our knowledge, there has been no systematic study of the effects of NP size on the polymer−polymer blends. For such a study, different NPs with controlled size and surface properties are required.

Figures 1a,b show TEM images of two different Au NPs used in this study and corresponding histograms of their size distributions. It was found that small Au NPs (Au NP-1) and large Au NPs (Au NP-2) have the average core diameters of 2.7 and 12.3 nm, respectively. To impart the thermal stability as well as the same surface chemistry to Au NPs, both types of Au NP were coated with polymeric ligands of thiol-terminated PS-*b*-PSN_3 polymers containing UV-cross-linkable PSN_3 blocks.[65] Because the polymeric shell was not visible in TEM due to insufficient contrast of the polymer ligands, the polymer shell thickness was estimated based on the Au core size, which was determined using TEM, and the relative weights of the Au core and the polymer ligands in the Au NPs, which were determined using TGA. To precisely estimate the polymeric shell thickness and the exact amount of grafted PS-*b*-PSN_3 ligands, it is critical to remove all ungrafted polymeric ligands from the polymer coated Au NPs. To accomplish this, the synthesized (PS-*b*-PSN_3)-Au NPs were washed several times using a density gradient method.[59,66] Any presence of ungrafted polymer ligands was monitored by SEC and TGA after each washing step to ensure their complete removal. The characteristics of two different (PS-*b*-PSN_3)-Au NPs are summarized in Table 2. It was found that the overall (polymer shell + Au core) diameter of small Au NP-1 is 5.9 nm and that the diameter of large Au NP-2 is 3.5 times larger (~20.7 nm). The parameter Σ, which is the areal chain density

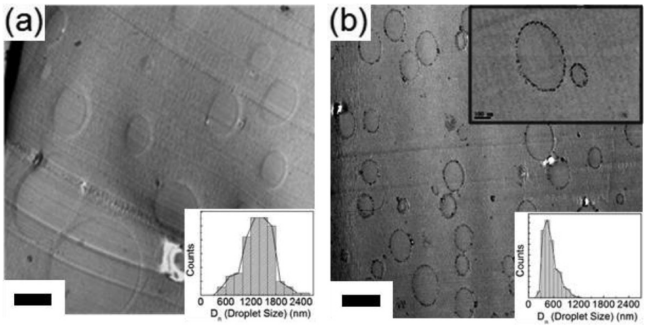

Figure 2. Cross-sectional TEM images showing PS/PTPA blends (a) without and (b) with the addition of 1.0 vol % Au NP-1 after thermal annealing for 48 h at 200 °C. Scale bar is 1 μm. The corresponding histograms (inset) show the PTPA droplet size within the PS matrix. Most of the Au NP-1 were segregated at the interface between PS and PTPA domains without any aggregation as shown in the magnified TEM image (inset; scale bar = 100 nm).

of the PS-*b*-PSN_3 chains on the Au NPs, is important in determining the enthalpic interaction between the NPs and the polymer matrix. For both Au NP-1 and Au NP-2, the value of Σ was estimated to be lower than 2 chains/nm^2; thus, in both cases, there was insufficient chain density to completely cover the Au NP surface.[48,67] The resulting Au NPs consist of nonpolar PS outer brushes and polar PSN_3 inner cross-linked shell. Therefore, it can be anticipated that the PS outer shell is compatible with the PS matrix, while the polar PSN_3 inner shell and bare Au NP surface can favorably interact with the polar PTPA matrix due to the presence of nitrogen in PTPA. It should be noted that due to the presence of azide cross-linkable block (PSN_3) as the shell on the particle surface, both Au NP-1 and Au NP-2 possess excellent thermal stability, which is a critical prerequisite for the use of Au NPs as compatibilizers in polymer blends that require high-temperature thermal processing above the T_g of both polymers. To verify their thermal stability, Au NP-1 and Au NP-2 were dissolved in dibutyl phthalate (DBP, bp = 340 °C), and thermal testing was carried out by heating the DBP solution to 150 °C for 24 h. Figures 1c,d show photographic images of Au NP-1 dissolved in DBP before and after heating; there is no evidence of aggregation of the PS-*b*-PSN_3 coated Au NPs. Figures 1e,f demonstrate the thermal stability of Au NP-2. The results indicate that both Au NP-1 and Au NP-2 are thermally stable and can be used in high-temperature processes, unlike traditional Au NPs that do not have cross-linked shells.

To investigate the effect of Au NPs on polymer blend morphology, two different samples of PS/PTPA blends (a volume ratio of PS/PTPA = 8/2), without and with the addition of 1.0 vol % Au NP-1, were prepared. Both samples were annealed at 200 °C for various annealing times under ultrahigh vacuum ($<10^{-6}$ Torr) to avoid oxidation or degradation. The PS/PTPA volume ratio of 8/2 in the blend was used because the morphology of macrophase-separated PTPA droplets in the PS matrix was consistently observed through the entire sample, as seen by the optical microscopy images (Figure S4). Because it is well-known that the dispersed domain size increases with annealing time because of the coalescence process,[68,69] the morphologies of both samples without and with Au NP-1 were observed as a function of annealing time. At the initial stage of annealing, the morphology of the PS/PTPA/Au NP-1 blend changed, indicated by a change in the droplet size of the PTPA

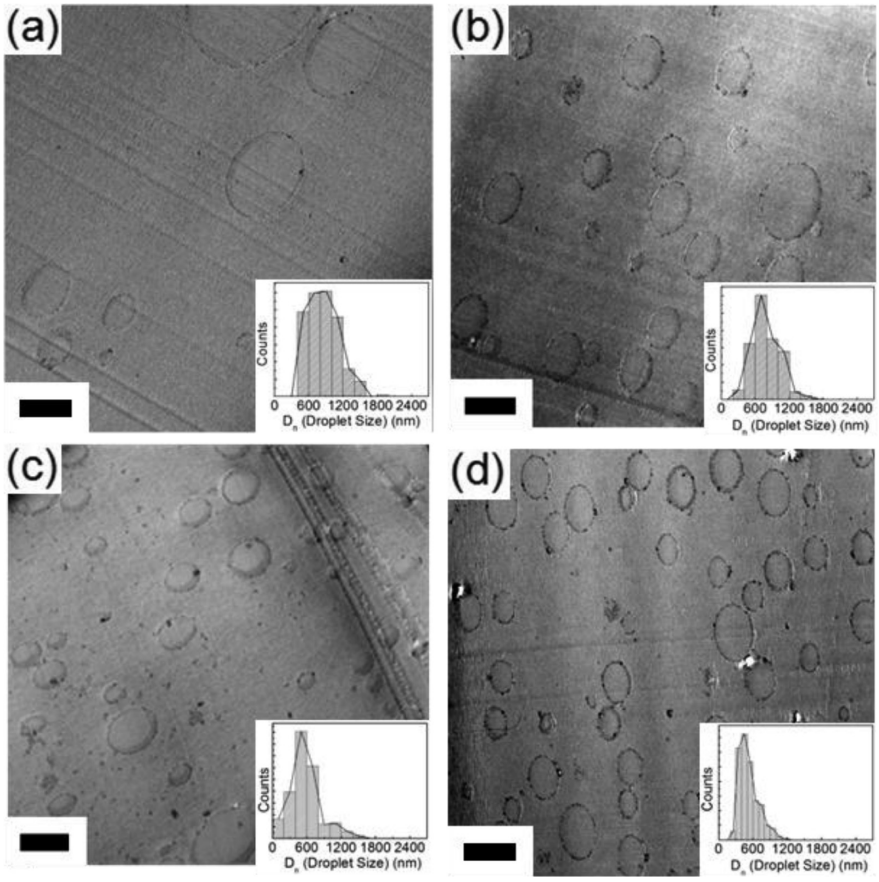

Figure 3. Cross-sectional TEM images of PS/PTPA blends containing Au NP-1 with the particle volume fractions (ϕ_p) of (a) 0.1, (b) 0.2, (c) 0.5, and (d) 1.0 vol % after thermal annealing at 200 °C for 48 h. Scale bar is 1 μm. The corresponding histograms (inset) represent the size distribution of the PTPA droplets within the PS matrix.

minor phase in the PS matrix. The morphology of the PS/PTPA blend was stabilized after annealing at 200 °C for 36 h, regardless of Au NP concentration. Based on this result, the annealing for 48 h at 200 °C was used to produce a stable morphology of the PS/PTPA blend and to monitor the effect of the addition of Au NPs on the blend morphology. Figure 2 shows cross-sectional TEM images of PS/PTPA blends (a) without and (b) with the addition of 1.0 vol % Au NP-1 after annealing at 200 °C for 48 h. Because of the immiscibility between the PS and PTPA phases, the morphology of the PS/PTPA blend showed two distinct domains: one consisting of droplets of one polymer and the other consisting of dispersed matrix. When the Au NPs were mixed with the PS/PTPA blend, a dramatic degree of localization of the Au NPs at the polymer/polymer interface was observed. This phenomenon can be explained by the existence of a balanced interaction between Au NPs and the PS/PTPA matrix, as mentioned previously. No aggregation was observed after thermal annealing, indicating excellent thermal stability of Au NP-1. Figure 2 shows the dramatic effect of Au NP compatibilizers on the blend morphology, which brings a significant reduction in the PTPA droplet size from 1.4 μm (without Au NP-1) to 500 nm (with 1 vol % Au NP-1).

To further confirm the compatibilizing effect of Au NP-1 on blend morphology, the morphology of PS/PTPA blends containing different volume fractions (ϕ_p) of Au NP-1 ranging from 0.1 to 1.0 vol % was investigated using cross-sectional TEM, as shown in Figure 3. All samples were prepared under the same conditions as described for the previous sample and were annealed at 200 °C for 48 h. To quantitatively analyze the compatibilizing effect of Au NPs, the number-average size (D_n) of PTPA droplets in the blend and their size distribution were obtained by analysis of TEM images, counting at least 300−400 units of droplets in each sample. The statistics are shown in the corresponding histograms as an inset in each figure. Regardless of ϕ_p, all Au NPs were segregated along the PS/PTPA interface, showing their compatibilizing effect. With the increase in the ϕ_p of Au NP-1, the amount of NPs segregated at the interface between the PS/PTPA phases also increased proportionally, with no particle aggregation in either phase. Specifically, with increases in ϕ_p from 0 to 1 vol %, D_n decreased progressively from 1400 nm (ϕ_p = 0) to 860 nm (ϕ_p = 0.1 vol %) to 520 nm (ϕ_p = 1.0 vol %). However, with further addition of Au NP-1 above 1.0 vol %, D_n did not decrease further.

To investigate the effects of the size of Au NPs on their ability to function as compatibilizers in a polymer blend, Au NP-2, which is 3.5 times larger than Au NP-1, was incorporated into the PS/PTPA blend. In these experiments, ϕ_p in the blend was varied from 0 to 5.0 vol %, and the samples were annealed at 200 °C for 48 h. Figure 4 shows cross-sectional TEM images of PS/PTPA blends containing Au NP-2 at ϕ_p ranging from 0.1 to 5.0 vol %. The TEM images reveal a dramatic degree of localization of Au NP-2 at the

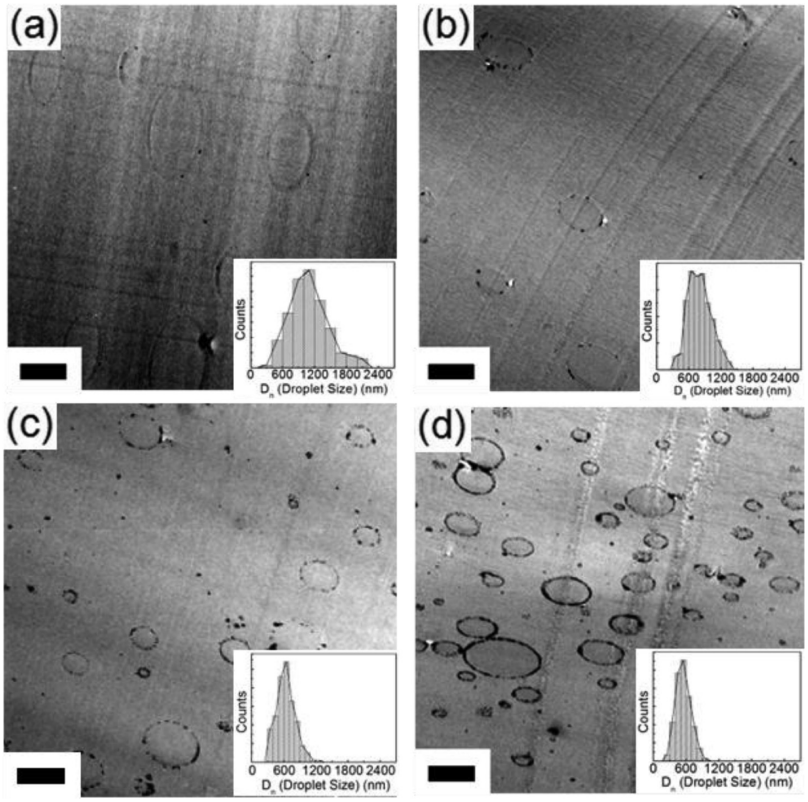

Figure 4. Cross-sectional TEM images of PS/PTPA blends containing Au NP-2 with volume fractions (ϕ_p) of (a) 0.1, (b) 0.5, (c) 1.0, and (d) 5.0 vol % after thermal annealing for 48 h at 200 °C. Scale bar is 1 μm. The corresponding histograms (inset) represent the size distributions of the PTPA droplets within the PS matrix.

PS/PTPA interface. Therefore, as ϕ_p increased from 0.1 to 5.0 vol %, the amount of Au NPs at the interface increased, causing a larger decrease in D_n. However, at low ϕ_p (<1.0 vol %), the change in D_n caused by the addition of Au NP-2 was much smaller than that by the addition of Au NP-1 at the same ϕ_p. As an example, the D_n value for PS/PTPA with Au NP-2 at ϕ_p = 1.0 vol % is larger (~700 nm) than the D_n value of 520 nm observed for the smaller Au NP-1 at the same ϕ_p.

To compare the compatibilizing effects of small-size Au NP-1 and large-size Au NP-2, D_n values were plotted as a function of ϕ_p for the two types of particles (Figure 5a). For both Au NP-1 and Au NP-2, D_n decreased as ϕ_p increased. However, D_n for the PS/PTPA/Au NP-2 blend decreased at a much slower rate than that for PS/PTPA/Au NP-1. Unlike the PS/PTPA/Au NP-1 blend, where D_n remained unchanged above 1.0 vol % Au NP-1, D_n in the PS/PTPA/Au NP-2 blend did not become saturated until a ϕ_p value of 3.0 vol %. Second, although the ϕ_p saturation point beyond which D_n remains unchanged is different for Au NP-1 and Au NP-2 particles, the ultimate D_n size that can be achieved is nearly the same (520 nm) for both NPs.

To gain a better understanding of the particle size effect on PS/PTPA blend morphology, the blend morphology and the arrangement of Au NPs at the PS/PTPA interface were investigated for ϕ_p of 1.0 and 5.0 vol %, as shown in Figures 5b–e. At ϕ_p = 1.0 vol %, both Au NPs were strongly segregated along the PS/PTPA interface, but their coverage at the interface was different. Whereas the PS/PTPA interface in Figure 5b was filled with a monolayer of closely packed Au NP-1 particles, only part of the PS/PTPA interface was occupied by Au NP-2 at the same ϕ_p. At 5.0 vol % Au NP-1, Figure 5d shows Au NPs located at the interface, which is an indication of immaculate adsorption of Au NPs. Interestingly, under these conditions, the Au NP-1 formed multilayers along the PS/PTPA interface with a broad interfacial width. However, the Au NPs trapped at the interface as part of the multilayer did not exhibit an increased compatibilization effect; the D_n value remained unchanged. In contrast, for Au NP-2, an increase in ϕ_p from 1.0 to 5.0 vol % (shown in Figures 5c,e) resulted in a proportional increase in coverage by Au NP-2 at the PS/PTPA interface; at 5.0 vol %, all the Au NP-2 particles were segregated at the interface as a monolayer (Figure 5e). Therefore, it can be regarded that the difference in ϕ_p dependence between Au NP-1 and Au NP-2 originated from the difference in the interfacial area between the PS/PTPA phases occupied by Au NP-1 and Au NP-2 at the same ϕ_p values. These results also show that compatibilizers in excess of what is required for monolayer formation do not significantly influence the miscibility of polymer blends.

One of the main advantages of particle surfactants over conventional compatibilizers (i.e., block and graft copolymers) is their quasi-irreversible adsorption to the polymer–polymer interface. Block copolymers, in contrast, are present within the homopolymer matrix as micelles and/or free chains, which form reversible equilibrium with those at the interface. The results shown in Figure 5 clearly indicated that regardless of ϕ_p, both Au NP-1 and Au NP-2 were highly segregated at the PS/PTPA interface with almost no particles located in either the PS or the PTPA matrix. The phenomenon can be explained by estimating the adsorption energy of the particles to the PS/PTPA interface (E_a) using

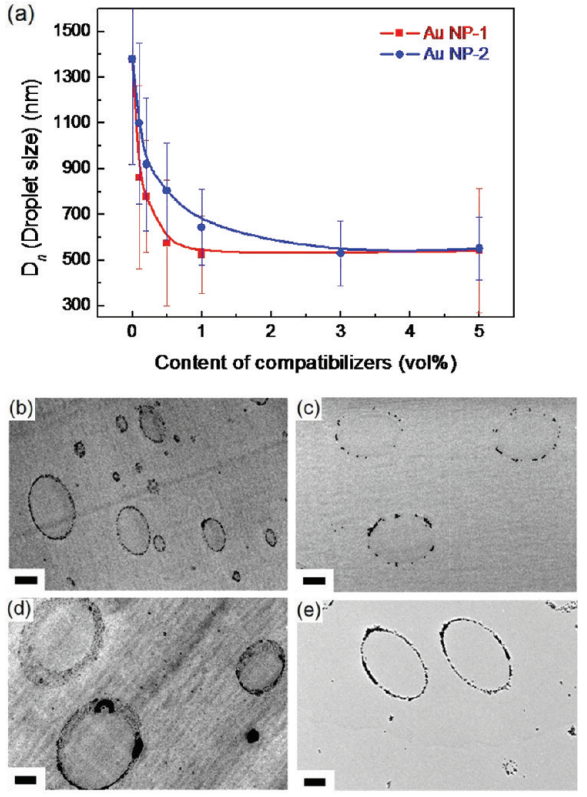

Figure 5. (a) Comparison of PTPA droplet sizes (D_n) as a function of ϕ_p for Au NP-1 and Au NP-2. Cross-sectional TEM images of PS/PTPA blends containing (b) Au NP-1 and (c) Au NP-2 with ϕ_p = 1.0 vol %. Panels d and e show TEM images of PS/PTPA blends containing (d) Au NP-1 and (e) Au NP-2 with ϕ_p = 5.0 vol %. Scale bar is 200 nm.

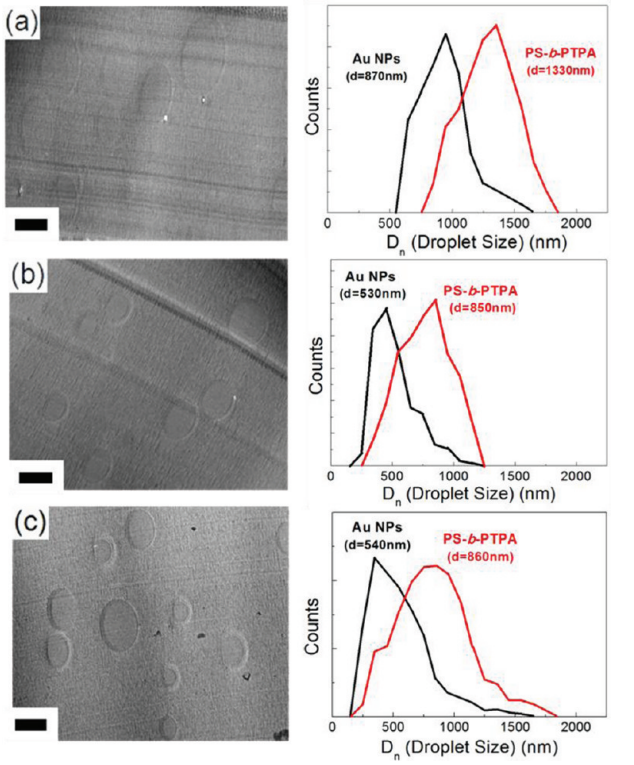

Figure 6. Cross-sectional TEM images of PS/PTPA blends containing symmetric PS-*b*-PTPA polymers with volume fractions (ϕ_{BC}) of (a) 0.1, (b) 1.0, and (c) 5.0 vol % after annealing for 48 h at 200 °C. Scale bar is 1 μm. The histograms on the right show a comparison of the statistical analysis of the PTPA droplets by two different compatibilizers of Au NP-1 and PS-*b*-PTPA at the same volume fraction.

the following equation:[41,64]

$$\frac{E_a}{k_B T} = \frac{\pi R^2 \gamma_{PS-PTPA}}{k_B T}(1 - |\cos(\theta)|)^2$$

$$\text{where } |\cos(\theta)| = \frac{|\gamma_{PS-NP} - \gamma_{PTPA-NP}|}{\gamma_{PS-PTPA}} \quad (1)$$

In eq 1, R is the radius of the Au NPs, and $\cos(\theta)$ is the ratio of the difference in interfacial tension between the NPs and two homopolymers to that between the PS and PTPA phases. For Au NP-1 (R = 2.95 nm) particles that are compatible with the PS and PTPA phases, $\cos(\theta) \ll 1$ and $E_a \approx \pi R^2 \gamma_{PS-PTPA}$, which should be much higher than $k_B T$. Furthermore, one can expect that there is a strong favorable enthalpic interaction between the bare Au surface and the nitrogen atoms in the PTPA polymer, and thus E_a is expected to be even higher. In addition, any tendency of the P(S-*b*-SN_3)-Au NP polymers to segregate in 2D on the NP surfaces would further favor particle adsorption.[35,42,70] Because E_a is proportional to R^2, E_a for large-size Au NP-2 should be 12.3 times larger than that for Au NP-1. Therefore, both particles are expected to be strongly bound to the PS/PTPA interface.

To demonstrate the effectiveness of Au NP compatibilizers, a comparison with existing polymer blend stabilizers is very desirable. Currently, block copolymers are state-of-the-art compatibilizers for polymer blends. Therefore, symmetric PS-*b*-PTPA diblock copolymers were synthesized by controlled radical polymerization of RAFT to be utilized as a control. The M_n of block copolymer compatibilizers is an important factor in determining their effectiveness as compatibilizers because low-M_n polymers are highly soluble in the homopolymer phases of the blend system, while high-M_n polymers tend to form micelle structures in the homopolymer phases.[33,71] Therefore, the M_n of the PS-*b*-PTPA used in this study was carefully chosen to produce a total M_n of 54 kg/mol where the PS block is 27 kg/mol. The calculated radius of gyration (R_g) was estimated to be 5.2 nm, which falls between the radii of Au NP-1 (2.95 nm) and Au NP-2 (10.35 nm). The phase behavior of PS-*b*-PTPA polymers was characterized by SAXS and SFM measurements (Figures S7 and S8), showing a lamellar morphology with a domain spacing of 23 nm. Therefore, a reasonable comparison between NP and block copolymer compatibilizers can be made using our synthesized PS-*b*-PTPA polymers.

Figure 6 shows cross-sectional TEM images of the PS/PTPA blends containing symmetric PS-*b*-PTPA polymers with volume fractions (ϕ_{BC}) of (a) 0.1, (b) 1.0, and (c) 5.0 vol % after annealing at 200 °C for 48 h. The histograms to the right of the TEM images show statistical analyses of the changes in D_n that resulted from the addition of Au NP-1 and PS-*b*-PTPA compatibilizers at a given compatibilizer volume fraction. The blend samples compatibilized by PS-*b*-PTPA block copolymers followed a similar trend of decreasing D_n with increasing ϕ_{BC}; however, for any given concentration of compatibilizer, the D_n was larger for PS/PTPA/PS-*b*-PTPA than for PS/PTPA/Au NP-1. For example, with the addition of 0.1 vol % PS-*b*-PTPA, D_n decreased from 1400 to 1330 nm, which is only a 5% decrease. By

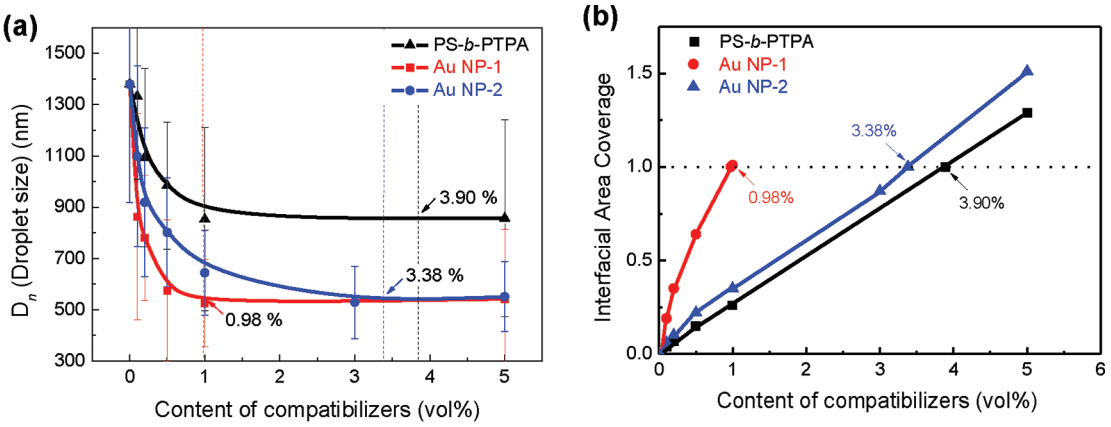

Figure 7. (a) Evolution of the PTPA droplet size (D_n) as a function of the compatibilizer volume fraction for PS-*b*-PTPA, Au NP-1, and Au NP-2. (b) The interfacial area coverage (A_C) by compatibilizers at the PS/PTPA interface was estimated as a function of the compatibilizer volume fraction for PS-*b*-PTPA, Au NP-1, and Au NP-2.

contrast, for the same volume fraction of Au NP-1, D_n decreased from 1400 to 870 nm (a 38% decrease), as shown in Figure 6a. Furthermore, for the PS-*b*-PTPA system, D_n became saturated at a much larger size of 900 nm at 1 vol % than in the Au NP-1 system (Figure 6b). From the saturated D_n values, the ratio of interfacial tension of the Au NPs blend to that of the PS-*b*-PTPA block copolymer blend can be estimated as ~0.58, assuming that the values of free energy for the systems are similar. Therefore, it can be concluded that Au NPs exhibit a much stronger compatibilizing effect.

The results shown in Figure 7a compare the three compatibilizers, Au NP-1, Au NP-2, and PS-*b*-PTPA, and summarize their effects on the blend morphology. According to the experimental results, Au NP-1 is the best compatibilizer. The blend system with Au NP-1 showed the lowest saturated concentration (ϕ_p ~1.0 vol %) and the smallest D_n, whereas the Au NP-2 compatibilized blend system had a saturated concentration ϕ_p of above 3.0 vol %. This difference in ϕ_p can be explained by the particle size effect. Another point to be noted is that whereas the saturated D_n values for Au NP-1 and Au NP-2 were almost identical, the block copolymers showed a unique dependence on saturated D_n size. Although the ϕ_{BC} at the saturation point (~1.0 vol %) in the block copolymer compatibilized blend system is similar to that for the Au NP-1 blend system, its saturated D_n was 1.8 times larger than for the Au NP blend system. To discuss the results more quantitatively, the interfacial coverage (A_C) of Au NPs was estimated using the following assumptions: (1) all of the Au NPs are located at the interface, and (2) the Au NPs form 2D monolayers hexagonally packed on the surfaces of the PTPA droplets. The A_C by the Au NPs can be estimated from the ratio of the effective total surface area occupied by the compatibilizers to the total surface area of the PTPA droplets, as in the following equation:

$$A_C = \frac{A_{AuNP}}{A_{interface}} = \frac{\pi(R_{AuNP})^2 N_{AuNP}}{4\pi(R_{PTPA})^2 N_{PTPA}} \frac{1}{0.91} \quad (2)$$

In eq 2, A_{AuNP} is the total effective area of the PTPA droplets covered by Au NPs; $A_{interface}$ is the total interfacial area between the PS and PTPA domains, which can be calculated from the total surface area of the PTPA droplets; R_{AuNP} and R_{PTPA} are the radii of the Au NPs and PTPA droplets, respectively, and N_{AuNP} and N_{PTPA} are the number of Au NPs and PTPA droplets in a given volume of the sample. Based on the A_C value, the amount of each compatibilizer required to produce saturation at the interface can be estimated. For PS-*b*-PTPA polymers, the coverage at the interface is calculated using the same method as for Au NPs, i.e., eq 2, for which the parameters for Au NPs are replaced with those for the PS-*b*-PTPA block copolymer. To estimate the area of the PS-*b*-PTPA block copolymer at the interface, it is assumed that the block copolymer forms two blobs that are composed of PS and PTPA blocks, respectively. Because, in the case of surfactants, the area of a surfactant molecule at the interface is usually determined by the area of a hydrophilic group,[72] the radius of a PTPA blob is used for calculation. When compatibilizer units partially enclose the interface, A_C is less than 1, whereas when excess compatibilizers are added to the blend system, A_C is greater than 1; additionally, when compatibilizers are fully saturated along the interface, the value of A_C is 1. The PS/PTPA interface is estimated to be fully covered by Au NP-1 at ϕ_p = 0.98 vol % and by Au NP-2 at ϕ_p = 3.38 vol %. The calculation predicts that the PS/PTPA interface will be saturated by PS-*b*-PTPA at ϕ_{BC} of 3.90%. For Au NP-1 and Au NP-2, the ϕ_p values for A_C = 1 show excellent agreement with those for D_n saturation point, as indicated by the red (Au NP-1) and blue (Au NP-2) dotted lines in Figures 7a,b. In contrast, the PS-*b*-PTPA concentration (ϕ_{BC} = 3.90 vol % at A_C = 1) is much higher than the actual D_n saturation point, which is ~1 vol %. This observation could be explained by the fact that many of the block copolymers were not localized at the interface due to micelle structure formation in the homopolymer phases.[73−77] In contrast, all Au NPs were strongly localized at the PS/PTPA interface. This difference makes our Au NPs better compatibilizers.

CONCLUSIONS

In this study, we systematically developed an efficient method for fabricating compatibilized polymer blends with a low concentration of Au NPs. Two different polymer-coated Au NPs with sizes of 5.9 and 20.7 nm were designed to be thermally stable above 200 °C and neutral to both the PS and PTPA phases. TEM images reveal that the polymer-coated Au NPs were perfectly localized on the surface of PTPA droplets, and no aggregation of Au NPs in either the PS or the PTPA domain was

observed. Therefore, both Au NPs function as effective compatibilizers in the PS/PTPA blend by inducing a dramatic reduction in D_n. To obtain the same amount of reduction in D_n, a higher ϕ_p was required for larger Au NP-2 than for small Au NP-1, demonstrating the size effect of Au-NPs on the blend morphology. At high concentration (ϕ_p = 5.0 vol %), small Au NP-1 exhibited a multilayered formation on the droplets, whereas a monolayered structure was observed for the blend using large Au NP-2. The estimated ϕ_p required to cover the interface with a monolayer agrees well with the experimental ϕ_p values for saturation of D_n for both small Au NP-1 and large Au NP-2. In contrast, the calculated ϕ_{BC} value for A_C = 1 in the PS-*b*-PTPA block copolymer compatibilizer system is much larger than the ϕ_p value for saturation of droplet size. In addition, the D_n value for the PS-*b*-PTPA system was saturated at 900 nm, which is much larger than 500 nm for both the Au NP-1 and the Au NP-2 systems. This different behavior could be mainly due to the formation of micelle structures of these compatibilizers in the homopolymer phase. Therefore, Au NPs exhibit a much stronger compatibilizing effect due to their dramatic localization at the PS/PTPA interface.

■ ASSOCIATED CONTENT

Supporting Information. Additional SEC, TGA, TEM, SAXS, and SFM data. This material is available free of charge via the Internet at http://pubs.acs.org.

■ AUTHOR INFORMATION

Corresponding Author
*E-mail: bumjoonkim@kaist.ac.kr.

■ ACKNOWLEDGMENT

This research was supported by the Korea Research Foundation Grant, funded by the Korean Government (2011-0017943, 2011-0027240, 2011-0027518). J.B. acknowledges the support by the Human Resources Development Program of KETEP grant (No. 20114010203070). W.B.L. acknowledges the support by the Human Resources Development of KETEP grant (No. 20114010203090)

■ REFERENCES

(1) Halls, J. J. M.; Walsh, C. A.; Greenham, N. C.; Marseglia, E. A.; Friend, R. H.; Moratti, S. C.; Holmes, A. B. *Nature* **1995**, *376* (6540), 498–500.
(2) Yu, G.; Gao, J.; Hummelen, J. C.; Wudl, F.; Heeger, A. J. *Science* **1995**, *270*, 1789–1791.
(3) Thompson, B. C.; Fréchet, J. M. J. *Angew. Chem., Int. Ed.* **2008**, *47* (1), 58–77.
(4) Cho, C. H.; Kang, H.; Kang, T. E.; Cho, H. H.; Yoon, S. C.; Jeon, M. K.; Kim, B. J. *Chem. Commun.* **2011**, *47* (12), 3577–3579.
(5) Lu, G. H.; Tang, H. W.; Huan, Y. A.; Li, S. J.; Li, L. G.; Wang, Y. Z.; Yang, X. N. *Adv. Funct. Mater.* **2010**, *20* (11), 1714–1720.
(6) Qiu, L. Z.; Lee, W. H.; Wang, X. H.; Kim, J. S.; Lim, J. A.; Kwak, D.; Lee, S.; Cho, K. *Adv. Mater.* **2009**, *21* (13), 1349–1353.
(7) Kumar, A.; Baklar, M. A.; Scott, K.; Kreouzis, T.; Stingelin-Stutzmann, N. *Adv. Mater.* **2009**, *21* (44), 4447–4451.
(8) Kim, K.-H.; Kang, H.; Nam, S. Y.; Jung, J.; Kim, P. S.; Cho, C.-H.; Lee, C.; Yoon, S. C.; Kim, B. J. *Chem. Mater.* **2011**, *23* (22), 5090–5095.
(9) Fredrickson, G. H.; Bates, F. S. *Eur. Phys. J. B* **1998**, *1* (1), 71–76.
(10) Hillmyer, M. A.; Maurer, W. W.; Lodge, T. P.; Bates, F. S.; Almdal, K. *J. Phys. Chem. B* **1999**, *103* (23), 4814–4824.
(11) Pernot, H.; Baumert, M.; Court, F.; Leibler, L. *Nature Mater.* **2002**, *1* (1), 54–58.
(12) Bates, F. S.; Maurer, W. W.; Lipic, P. M.; Hillmyer, M. A.; Almdal, K.; Mortensen, K.; Fredrickson, G. H.; Lodge, T. P. *Phys. Rev. Lett.* **1997**, *79* (5), 849.
(13) Macosko, C. W.; Guégan, P.; Khandpur, A. K.; Nakayama, A.; Marechal, P.; Inoue, T. *Macromolecules* **1996**, *29* (17), 5590–5598.
(14) Park, D. W.; Roe, R. J. *Macromolecules* **1991**, *24* (19), 5324–5329.
(15) Anastasiadis, S. H.; Gancarz, I.; Koberstein, J. T. *Macromolecules* **1989**, *22* (3), 1449–1453.
(16) Leibler, L. *Makromol. Chem., Macromol. Symp.* **1988**, *16* (1), 1–17.
(17) Noolandi, J.; Hong, K. M. *Macromolecules* **1984**, *17* (8), 1531–1537.
(18) Semenov, A. N. *Macromolecules* **1992**, *25* (19), 4967–4977.
(19) Williams, J. M.; Gray, A. J.; Wilkerson, M. H. *Langmuir* **1990**, *6* (2), 437–444.
(20) Binks, B. P. *Curr. Opin. Colloid Interface Sci.* **2002**, *7* (1−2), 21–41.
(21) Philipse, A. P.; Sacanna, S.; Kegel, W. K. *Phys. Rev. Lett.* **2007**, *98* (15), 158301.
(22) Kang, D. J.; Kwon, T.; Kim, M. P.; Cho, C.-H.; Jung, H.; Bang, J.; Kim, B. J. *ACS Nano* **2011**, *5* (11), 9017–9027.
(23) Silverstein, M. S.; Gurevitch, I. *J. Polym. Sci., Part A: Polym. Chem.* **2010**, *48* (7), 1516–1525.
(24) Colver, P. J.; Colard, C. A. L.; Bon, S. A. F. *J. Am. Chem. Soc.* **2008**, *130* (50), 16850–16851.
(25) Menner, A.; Ikem, V.; Salgueiro, M.; Shaffer, M. S. P.; Bismarck, A. *Chem. Commun.* **2007**, *41*, 4274–4276.
(26) Ikem, V. O.; Menner, A.; Bismarck, A. *Angew. Chem., Int. Ed.* **2008**, *47* (43), 8277–8279.
(27) Chen, T.; Colver, P. J.; Bon, S. A. F. *Adv. Mater.* **2007**, *19* (17), 2286–2289.
(28) Elias, L.; Fenouillot, F.; Majeste, J. C.; Cassagnau, P. *Polymer* **2007**, *48* (20), 6029–6040.
(29) Vo, L. T.; Giannelis, E. P. *Macromolecules* **2007**, *40* (23), 8271–8276.
(30) Elias, L.; Fenouillot, F.; Majeste, J. C.; Alcouffe, P.; Cassagnau, P. *Polymer* **2008**, *49* (20), 4378–4385.
(31) Gubbels, F.; Jerome, R.; Teyssie, P.; Vanlathem, E.; Deltour, R.; Calderone, A.; Parente, V.; Bredas, J. L. *Macromolecules* **1994**, *27* (7), 1972–1974.
(32) Chung, H.; Ohno, K.; Fukuda, T.; Composto, R. J. *Nano Lett.* **2005**, *5* (10), 1878–1882.
(33) Walther, A.; Matussek, K.; Muller, A. H. E. *ACS Nano* **2008**, *2* (6), 1167–1178.
(34) Li, L.; Miesch, C.; Sudeep, P. K.; Balazs, A. C.; Emrick, T.; Russell, T. P.; Hayward, R. C. *Nano Lett.* **2011**, *11* (5), 1997–2003.
(35) Shan, J.; Nuopponen, M.; Jiang, H.; Viitala, T.; Kauppinen, E.; Kontturi, K.; Tenhu, H. *Macromolecules* **2005**, *38* (7), 2918–2926.
(36) Corbierre, M. K.; Cameron, N. S.; Sutton, M.; Mochrie, S. G. J.; Lurio, L. B.; Ruhm, A.; Lennox, R. B. *J. Am. Chem. Soc.* **2001**, *123* (42), 10411–10412.
(37) Kang, H.; Detcheverry, F. A.; Mangham, A. N.; Stoykovich, M. P.; Daoulas, K. C.; Hamers, R. J.; Muller, M.; de Pablo, J. J.; Nealey, P. F. *Phys. Rev. Lett.* **2008**, *100* (14), 148303.
(38) Bockstaller, M. R.; Mickiewicz, R. A.; Thomas, E. L. *Adv. Mater.* **2005**, *17* (11), 1331–1349.
(39) Oh, H.; Green, P. F. *Nature Mater.* **2009**, *8* (2), 139–143.
(40) Kim, B. J.; Bang, J.; Hawker, C. J.; Kramer, E. J. *Macromolecules* **2006**, *39* (12), 4108–4114.
(41) Chiu, J. J.; Kim, B. J.; Kramer, E. J.; Pine, D. J. *J. Am. Chem. Soc.* **2005**, *127* (14), 5036–5037.
(42) Kim, B. J.; Bang, J.; Hawker, C. J.; Chiu, J. J.; Pine, D. J.; Jang, S. G.; Yang, S. M.; Kramer, E. J. *Langmuir* **2007**, *23* (25), 12693–12703.

(43) Li, C.; Han, J.; Ryu, C. Y.; Benicewicz, B. C. *Macromolecules* **2006**, *39* (9), 3175–3183.
(44) Bockstaller, M. R.; Lapetnikov, Y.; Margel, S.; Thomas, E. L. *J. Am. Chem. Soc.* **2003**, *125* (18), 5276–5277.
(45) He, J. B.; Tangirala, R.; Emrick, T.; Russell, T. P.; Boker, A.; Li, X. F.; Wang, J. *Adv. Mater.* **2007**, *19* (3), 381–385.
(46) Wang, W. P.; Cao, H. M.; Zhu, G. J.; Wang, P. *J. Polym. Sci., Part A: Polym. Chem.* **2010**, *48* (8), 1782–1790.
(47) Paek, K.; Chung, S.; Cho, C. H.; Kim, B. J. *Chem. Commun.* **2011**, *47* (37), 10272–10274.
(48) Jang, S. G.; Khan, A.; Dimitriou, M. D.; Kim, B. J.; Lynd, N. A.; Kramer, E. J.; Hawker, C. J. *Soft Matter* **2011**, *7* (13), 6255–6263.
(49) Kim, B. J.; Fredrickson, G. H.; Hawker, C. J.; Kramer, E. J. *Langmuir* **2007**, *23* (14), 7804–7809.
(50) Hawker, C. J.; van Berkel, K. Y. *J. Polym. Sci., Part A: Polym. Chem.* **2010**, *48* (7), 1594–1606.
(51) Yoo, M.; Kim, S.; Lim, J.; Kramer, E. J.; Hawker, C. J.; Kim, B. J.; Bang, J. *Macromolecules* **2010**, *43* (7), 3570–3575.
(52) Al Akhrass, S.; Damiron, D.; Carrot, G.; Drockenmuller, E. *J. Polym. Sci., Part A: Polym. Chem.* **2010**, *48* (17), 3888–3895.
(53) Drockenmuller, E.; Li, L. Y. T.; Ryu, D. Y.; Harth, E.; Russell, T. P.; Kim, H. C.; Hawker, C. J. *J. Polym. Sci., Part A: Polym. Chem.* **2005**, *43* (5), 1028–1037.
(54) Perrier, S.; Takolpuckdee, P. *J. Polym. Sci., Part A: Polym. Chem.* **2005**, *43* (22), 5347–5393.
(55) Monteiro, M. J. *J. Polym. Sci., Part A: Polym. Chem.* **2005**, *43* (22), 5643–5651.
(56) Boyer, C.; Stenzel, M. H.; Davis, T. P. *J. Polym. Sci., Part A: Polym. Chem.* **2011**, *49* (3), 551–595.
(57) Lim, J.; Yang, H.; Paek, K.; Cho, C.-H.; Kim, S.; Bang, J.; Kim, B. J. *J. Polym. Sci., Part A: Polym. Chem.* **2011**, *49* (16), 3464–3474.
(58) Brust, M.; Walker, M.; Bethell, D.; Schiffrin, D. J.; Whyman, R. *J. Chem. Soc., Chem. Commun.* **1994**, *7*, 801–802.
(59) Kwon, T.; Min, M.; Lee, H.; Kim, B. J. *J. Mater. Chem.* **2011**, *21*, 11956–11960.
(60) Frens, G. *Nature (London), Phys. Sci.* **1973**, *241* (105), 20–22.
(61) Trombly, D. M.; Ganesan, V. *J. Chem. Phys.* **2010**, *133* (15), 154904.
(62) Pryamitsyn, V.; Ganesan, V. *Macromolecules* **2006**, *39* (24), 8499–8510.
(63) Horozov, T. S.; Binks, B. P. *Angew. Chem., Int. Ed.* **2006**, *45* (5), 773–776.
(64) Pieranski, P. *Phys. Rev. Lett.* **1980**, *45* (7), 569–572.
(65) Büttner, M.; Belser, T.; Oelhafen, P. *J. Phys. Chem. B* **2005**, *109* (12), 5464–5467.
(66) Bai, L.; Ma, X. J.; Liu, J. F.; Sun, X. M.; Zhao, D. Y.; Evans, D. G. *J. Am. Chem. Soc.* **2010**, *132* (7), 2333–2337.
(67) Kim, B. J.; Fredrickson, G. H.; Kramer, E. J. *Macromolecules* **2008**, *41* (2), 436–447.
(68) Kim, J.; Gray, M. K.; Zhou, H.; Nguyen, S. T.; Torkelson, J. M. *Macromolecules* **2005**, *38* (4), 1037–1040.
(69) Lee, M. S.; Lodge, T. P.; Macosko, C. W. *J. Polym. Sci., Part B: Polym. Phys.* **1997**, *35* (17), 2835–2842.
(70) Folkers, J. P.; Laibinis, P. E.; Whitesides, G. M. *Langmuir* **1992**, *8* (5), 1330–1341.
(71) Israels, R.; Jasnow, D.; Balazs, A. C.; Guo, L.; Krausch, G.; Sokolov, J.; Rafailovich, M. *J. Chem. Phys.* **1995**, *102* (20), 8149–8157.
(72) Rosen, M. J. *Frontmatter, in Surfactants and Interfacial Phenomena*, 3rd ed., John Wiley & Sons, Inc.: Hoboken, NJ, USA, 2004.
(73) Maric, M.; Macosko, C. W. *J. Polym. Sci., Part B: Polym. Phys.* **2002**, *40* (4), 346–357.
(74) Braun, D.; Fischer, M.; Hellmann, G. P. *Polymer* **1996**, *37* (17), 3871–3877.
(75) Auschra, C.; Stadler, R.; Voigtmartin, I. G. *Polymer* **1993**, *34* (10), 2081–2093.
(76) Shull, K. R.; Kramer, E. J. *Macromolecules* **1990**, *23* (22), 4769–4779.
(77) Shull, K. R.; Winey, K. I.; Thomas, E. L.; Kramer, E. J. *Macromolecules* **1991**, *24* (10), 2748–2751.